Rapid-phase modulation of terahertz radiation for high-speed terahertz imaging and spectroscopy

Alexander M. Sinyukov,[1] Zhiwei Liu,[1] Yew Li Hor,[1] Ke Su,[1] Robert B. Barat,[2] Dale E. Gary,[1] Zoi-Heleni Michalopoulou,[3] Ivan Zorych,[3] John F. Federici,[1,*] and David Zimdars[4]

[1]*Department of Physics, New Jersey Institute of Technology, Newark, New Jersey 07102, USA*
[2]*Otto York Department of Chemical Engineering, New Jersey Institute of Technology, Newark, New Jersey 07102, USA*
[3]*Department of Mathematical Sciences, New Jersey Institute of Technology, Newark, New Jersey 07102, USA*
[4]*Picometrix, 2925 Boardwalk, Ann Arbor, Michigan 48113, USA*
[*]*Corresponding author: federici@adm.njit.edu*

Received April 18, 2008; revised June 9, 2008; accepted June 15, 2008;
posted June 18, 2008 (Doc. ID 95170); published July 11, 2008

Rapid voltage-controlled phase modulation of cw terahertz (THz) radiation is demonstrated. By transmitting an infrared beam through a lithium niobate phase modulator the phase of the THz radiation, which is generated by the photomixing of two infrared beams, can be directly modulated through a 2π phase shift. The 100 kHz modulation rate that is demonstrated with this technique is approximately 3 orders of magnitude faster than what can be achieved by mechanical scanning. © 2008 Optical Society of America

OCIS codes: 120.5060, 300.6495, 110.6795.

Terahertz (THz) radiation has shown potential in a wide variety of applications, including detection of concealed weapons and explosives [1,2], chemical detection and spectroscopy [3], and imaging [4]. The feasibility of various THz applications has been greatly expanded owing to the development of spectroscopy and imaging methods such as THz time-domain spectroscopy (THz TDS) and cw THz imaging. One of the limitations in applying THz TDS to imaging has been the requirement for a scanning method that records the entire THz time-domain waveform [4]. Most time-domain THz systems use slow mechanical scanning delay lines, or mirror shakers (15–300 Hz repetition rate) [4], to detect the THz waveform on a point-by-point basis. Improvements to the mechanical scanning method have included piezoelectric delay lines, which are reasonably fast (kilohertz) but are limited to a 10 ps scanning range, as well as a rotating scanning stage [5].

For the cw photomixing configuration two laser sources are typically multiplied or mixed in a device such as a photoconductive antenna structure. THz radiation is generated at the difference frequency of the two laser sources. Some groups have used Golay cells, bolometers [6], or other power detection devices. Since the THz power, not the electric field, is detected in these devices, the THz phase information is lost. However, no scanning of the THz waveform is required. For the coherent detection approach, the THz waveform is scanned by varying the phase (or arrival) of the THz waveform relative to the phase of the mixed laser beams. Following the example of THz TDS, a mechanically scanning delay rail [7–9] typically is used to vary the optical path of the two infrared laser beams after the beams have been combined. These delay rails are typically slow, not because a long waveform is recorded (as is the case of the THz TDS systems), but rather because the delay induced by the scanning rail must be comparable in distance to the wavelength of the THz radiation (~300 μm for 1 THz). The rate of the scanning, however, can be increased by recognizing that the initial phase of the THz wave in the photomixing process is determined by the phase difference of the two lasers. We directly modulate the phase of one of the infrared lasers using an optoelectronic lithium niobate phase modulator. Since the speed of lithium niobate modulators can be as high as the gigahertz range, we essentially can eliminate the speed limitations due to mechanical scanning in acquiring a THz waveform.

The experimental setup for rapid cw detection of the THz phase and amplitude is presented in Fig. 1. THz radiation is generated at the beating frequency of two Littman external-cavity diode lasers (ECDLs,

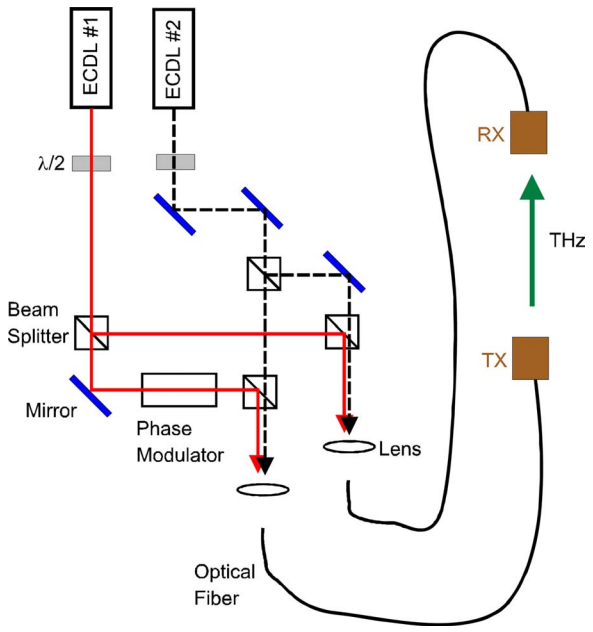

Fig. 1. (Color online) Schematic diagram of fast phase modulation configuration. The half-wave plates are used to rotate the polarization of the laser beams parallel to the polarization axis of the optical fibers.

 © 2008 Optical Society of America

Sacher Lion TEC520) operating near 0.78 μm. For these experiments they are detuned by 0.6 nm, which corresponds to 0.3 THz. The output of each laser is evenly split using the first pair of beam splitters. The $MgO:LiNbO_3$ phase modulator (New Focus 4002) is inserted into one of the beams from ECDL 1. After splitting and passing one beam through the modulator, the light from the two lasers is combined with another pair of beam splitters. The combined laser light is coupled into polarization maintaining optical fibers and delivered to both the THz transmitter (TX) and receiver (RX). The TX and RX are low-temperature-grown GaAs bowtie-type photoconductive dipole antennae (PDA). The total optical power on both channels is ~12 mW. A bias of 20 V dc is applied to power the THz TX. For the portion of the system that operates in free space (~47 cm), beam walk of the lasers does not appear to play a major role. As the wavelength of either ECDL is piezotuned, we observe <3% fluctuation in the polarized optical power that emerges from the optical fibers.

THz radiation is generated by photomixing of the two laser beams in the THz TX. The generated THz wave can be presented as a product of electric fields, $E_{\mathrm{THz}} \sim \mathbf{E_1} \cdot \mathbf{E_2} \sim E_1 E_2[\cos(\Delta\omega t + \Delta\phi_0)]$, where $\Delta\omega = \omega_1 - \omega_2$, $\Delta\phi_0 = \phi_1 - \phi_2$, E_1 and E_2 are the amplitudes of infrared EDCL electric fields at the frequencies ω_1 and ω_2, and phases ϕ_1 and ϕ_2, respectively. The electro-optic phase modulator, which is inserted into the optical path of the ECDL 1 beam that will drive the THz transmitter, is oriented so that the applied voltage induces a change in refractive index along the polarization axis of the infrared laser beam. By varying the applied voltage to the phase modulator, the optical path length experienced by the propagating laser beam varies proportionally. Adding the additional phase shift $\phi_m(t)$ induced by the modulator gives $E_{\mathrm{THz}}(t) \sim E_1 E_2[\cos(\Delta\omega t + \Delta\phi_0 + \phi_m(t))]$, where the time-dependent phase shift can be expressed as $\phi_m(t) = C_o V(t)$, in which C_o is a constant and $V(t)$ is the applied voltage. Since the phase shift is proportional to the applied voltage, a linear phase shift requires a linear increase in voltage. After passing through free space to the THz detector, the THz beam acquires a phase shift of ϕ_p. The detected THz signal is determined by mixing (multiplying) the incoming THz radiation with the two infrared ECDL signals present at the THz detector: $E_{\mathrm{det}}(t) \sim E_1^2 E_2^2 \cos(\phi_m(t) + \phi_p)$.

The output of the THz receiver can be recorded with a digital lock-in amplifier that locks to the ramp modulation frequency. However, if the voltage swing corresponds to a phase shift that was either smaller than or larger than 2π, the output voltage from the THz RX would not be perfectly sinusoidal. The need for a complete 2π phase shift in the modulator is illustrated in Fig. 2. For voltages below the equivalent of a 2π phase shift, the output waveforms [Fig. 2(a)] are not complete sinusoids. For voltages that are too large [Fig. 2(b)], a waveform swing larger than one cycle is observed. The infrared wavelength of ECDL 1 in Fig. 1 is kept fixed while the wavelength of ECDL 2 is tuned to vary the THz wavelength. In this case, the required voltage for a 2π phase shift should remain fixed.

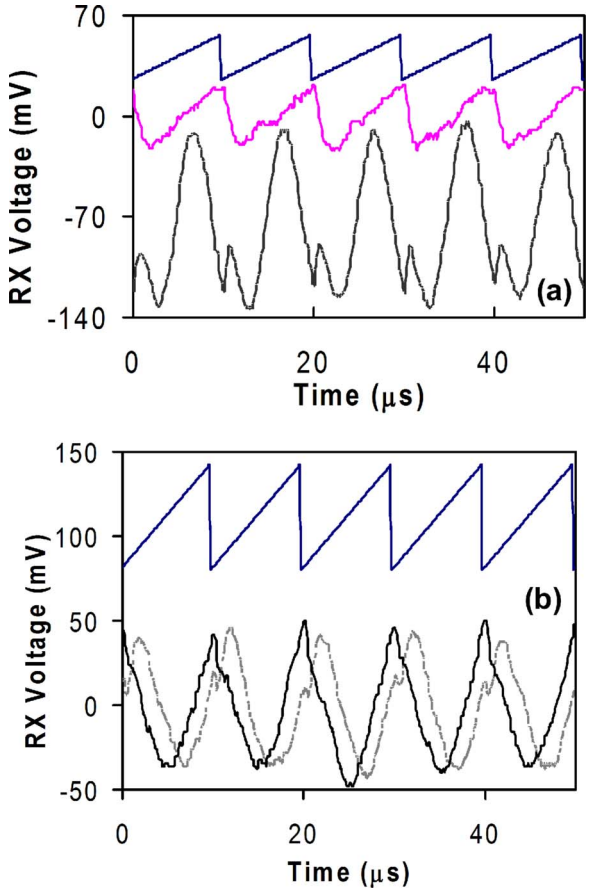

Fig. 2. (Color online) THz detector voltage output versus time as a function of applied voltage to the modulator. (a) The applied voltage is 20 and 160 V (middle and bottom waveforms, respectively). The sawtooth waveform (top) illustrates the timing of the modulator voltage. Waveforms are vertically offset for clarity. (b) THz detector output for a thin card inserted (solid curve) between the THz TX and RX of Fig. 1 and removed (dashed curve).

When an object is inserted between the THz TX and RX, which modifies the phase shift of the propagating THz beam ϕ_p, the measured phase of the RX waveform shifts as well. To illustrate this effect we insert a thin business card between the THz TX and RX of Fig. 1. When the phase modulator voltage is set correctly, the phase of the THz RX waveform shifts by 1.6 μs, corresponding to a 0.32π phase shift of the THz wave [Fig. 2(c)]. If we neglect any birefringence in the paper the measured phase shift for the 0.34 mm thick card corresponds to a 1.47 index of refraction. The kinks in the waveforms at 0, 10, 20, 30, and 40 ps correspond to the ramp voltage resetting from a 2π to a 0π phase shift. With the card present the kink occurs almost at the peak of the waveform, while the kink occurs about halfway up the waveform when the card is removed.

To demonstrate the utility of the method for fast spectral scanning we utilize the piezotuning capabilities on ECDL 2 to sweep the THz frequency. Figure 3 illustrates the measured THz amplitude and phase

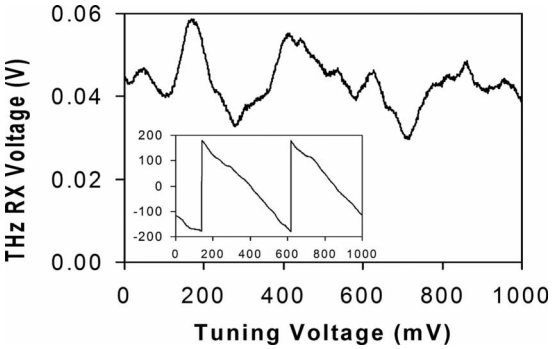

Fig. 3. Rapid frequency tuning curves for the measured THz amplitude and phase in degrees (inset) over ~3 GHz.

as measured with a digital lock-in amplifier using a time constant of 640 μs. For this measurement the total tuning range of 1 V corresponds to a tuning of the THz frequency by ~3 GHz. Over this range of tuning the laser does not exhibit any mode hops. The THz is scanned at 3 MHz per data point, which corresponds roughly to the spectral width of the ECDL. The acquisition time for the 1000 data point scan of Fig. 3 is completed in only a few seconds.

The Fig. 3 inset shows the measured change in phase during tuning. Ideally, if the optical path lengths for ECDL 2 through the optical components and fiber-optical cables to the TX and RX were identical, there would be no observed change in phase with frequency. Based on the measured 2π phase shift over 1.43 GHz, we estimate a path difference of roughly 21 cm. This distance corresponds roughly to the expected optical path length delay due to mismatched optical fiber lengths in our system.

In regard to cw THz systems with mechanical scanning of the THz waveform, the 100 kHz repetition rate is roughly 3 orders of magnitude faster. The maximum scanning speed of the current system is limited by the electronic bandwidth (roughly 420 kHz) of the THz RX. In a classic THz imaging configuration in which the object's position is scanned between a single THz TX and RX, the rapid-scanning system operating at 100 kHz will enable an averaging of 100 oscillations of the THz waveform with roughly 1000 pixels imaged per second. If synthetic aperture imaging methods [10] were utilized, video-rate imaging would be attainable.

In applying THz spectroscopy to the gas phase chemical detection, it has been recognized that the spectral width of the absorption lines of low pressure gases is about 1 MHz in the THz range. THz spectroscopy instrumentation for gas analysis includes a fast-scanning cavity ringdown approach [3] that enables the measurement of 6000 different THz frequencies at a rate of ~2000 data points per second. The data shown in Fig. 3 were acquired at a rate of ~1000 data points per second with a time constant of ~640 μs per data point. The ECDL's specification for the maximum rate of piezoactuated frequency tuning is 12 kHz. Consequently, the rapid phase modulation system should enable a data rate of ~12 k data points per second with a time constant of ~0.08 ms.

The authors gratefully acknowledge the funding assistance of the U.S. Army (Picattiny Arsenal). Insightful discussions with J. M. Joseph and L. Moller are acknowledged.

References

1. J. F. Federici, D. Gary, R. Barat, and Z.-H. Michalopoulou, in *Counter-Terrorism Detection Techniques of Explosives*, Jehuda Yinon, ed. (Elsevier, 2007).
2. T. Löffler, T. May, C. am Weg, A. Alcin, B. Hils, and H. G. Roskos, Appl. Phys. Lett. **90**, 091111 (2007).
3. A. I. Meshkov and F. C. De Lucia, Rev. Sci. Instrum. **76**, 083103 (2005).
4. W. L. Chan, J. Deibel, and D. M. Mittleman, Rep. Prog. Phys. **70**, 1325 (2007).
5. J. Xu and X.-C. Zhang, Opt. Lett. **29**, 2082 (2004).
6. J.-Y. Lu, H.-H. Chang, L.-J. Chen, M.-C. Tien, and C.-K. Sun, IEEE Photon. Technol. Lett. **17**, 2406 (2005).
7. A. Nahata, J. T. Yardley, and T. F. Heinz, Appl. Phys. Lett. **75**, 2524 (1999).
8. K. J. Siebert, H. Quast, R. Leonhardt, T. Loffler, M. Thomson, T. Bauer, H. G. Roskos, and S. Czasch, Appl. Phys. Lett. **80**, 3003 (2002).
9. N. Karpowicz, H. Zhong, J. Xu, K-I Lin, J-S Hwang, and X-C Zhang, Semicond. Sci. Technol. **20**, 293 (2005).
10. A. Bandyopadhyay, A. Stepanov, B. Schulkin, M. D. Federici, A. Sengupta, D. Gary, J. F. Federici, R. Barat, Z.-H. Michalopoulou, and D. Zimdars, J. Opt. Soc. Am. A **23**, 1168 (2006).